Hindawi
International Journal of Distributed Sensor Networks
Volume 2024, Article ID 6684449, 12 pages
https://doi.org/10.1155/2024/6684449

Research Article

Estimation of Joint Parameters Using Frequency-Based Substructuring Techniques

Hye-Sook Jang, Jae-Hyoung An, and Hee-Chang Eun

Department of Architectural Engineering, Kangwon National University, Chuncheon, Republic of Korea

Correspondence should be addressed to Hee-Chang Eun; heechang@kangwon.ac.kr

Received 29 November 2023; Revised 13 February 2024; Accepted 14 February 2024; Published 26 February 2024

Academic Editor: Yuedong Xie

This study presents frequency-based substructuring (FBS) techniques and an identification method for predicting joint parameters. Two FBS techniques, FBS-1 and FBS-2, were derived by assuming pseudomasses at the joint nodes between adjacent substructures. It is estimated that the main reason for the discrepancy with the analytical FRFs is the difficulty in describing the low-frequency responses owing to the assumed pseudomasses of the substructures. Although the FRF curve based on the FBS-2 technique is very close to the analytical FRF curve up to the first resonance frequency, some inconsistencies occur thereafter. It is analyzed that the FRFs up to the first resonance frequency can be utilized for data expansion methods and system identification techniques. Paying attention to this result, this study also provides an identification method to estimate the joint parameters based on the FRF variation. Its validity is illustrated using a numerical example.

1. Introduction

Employing dynamic substructuring techniques in the analysis of large structures can save time and cost by disassembling and synthesizing them into multiple substructures. The decoupled substructures are synthesized by applying deformation compatibility conditions to the common nodes between adjacent substructures. The substructures are brought into equilibrium by the generated interface forces to satisfy the constraint conditions. Existing structural synthesis techniques are divided into three types: component mode synthesis (CMS), frequency-based substructuring (FBS), and impulse-based substructuring (IBS) techniques. The CMS method simplifies complicated finite element models to reduced-order models, the FBS method assembles the frequency response functions (FRFs) of individual substructures, and the IBS method allows high-frequency dynamics.

FBS techniques obtain the FRFs of the entire system by assembling the numerical or experimental FRFs [1] of multiple substructures. There has been some difficulty in obtaining complete response datasets, including rotational responses, from experimental data. Silva and Maia [2, 3] estimated rotational FRFs by expanding measured FRFs based on modified Kidder's method and the principle of reciprocity. Batista and Maia [4] proposed a method to estimate rotational FRFs that cannot be measured. Wan Iskandar Mirza et al. [5] derived the translational and rotational FRFs from the experimental modal model using the finite element model reduction and expansion method. Hosoya and Yoshimura [6] estimated rotational FRFs by the inner force and the response of the connection point including rotational DOFs. Many updating techniques based on the measured FRFs have been proposed [7–12]. Patil [13] determined the joint parameters of the rotational and translational stiffness for connected systems using the modal coupling method of sensitivity modes. Drozg et al. [14] expanded the rotational degrees of freedom (DOFs) of an FRF matrix based on a modal model by introducing a Lagrange multiplier frequency-based substructuring (LM-FBS) technique. De Klerk et al. [15] introduced the LM-FBS method to improve the classical FBS method for assembling the dynamic admittance of substructures. Mahmoudi et al. [16] used the LM-FBS algorithm to treat flexible joints as substructures, presenting three approaches for avoiding the singularity problem in coupling substructures. Bouslema

et al. [17] investigated the global dynamic behavior of a coupled transmission system based on a double-reducer stage. By combining the position-invariant component-level receptances at the joint nodes between substructures, Law and Ihlenfeldt [18] introduced an FBS approach.

Estimating the stiffness and damping of joints between structural members, or between members and boundary points, is a topic of interest. Considering the continuity of load transfer, the stiffness of joints is an important factor in structural design and analysis. This can be estimated using the FRFs, including the dynamic characteristics of the structure. Jalali [19] proposed an identification method for predicting the stiffness of contact interfaces using linear interface parameters. Yang et al. [20] proposed multiobjective optimization algorithms to identify joint parameters from the relationship between joint parameter perturbation and structural dynamics. Sanati et al. [21] provided two identification approaches for the inverse receptance coupling method and an analytical joint identification approach to obtain the linear stiffness and damping of a joint. Yang et al. [22] identified joint parameters using the substructure synthesis approach, FRFs, and only two measurement points in the experiment. Lee and Hwang [23] derived an FBS technique by minimizing the difference between the reference and calculated responses and identified the joint parameters. By estimating the unmeasured FRFs from the measured FRFs, Yang and Park [24] identified the joint parameters using subset FRFs. Hwang [25] proposed an identification method for connections using FRFs by calculating and averaging the connection properties for each frequency. Li [26] presented a model-updating method for identifying joint stiffness using a reduced-order characteristic polynomial. The FBS techniques presented above introduced numerical schemes rather than explicit mathematical forms. The FBS techniques and identification approaches introduced above have limitations in research based on numerical analysis schemes.

This paper presents FBS techniques using compatibility conditions based on the FRF in the frequency domain and discusses their limitations. Assuming pseudomasses at the joint nodes between independent substructures, two FBS techniques are presented depending on the performance indices using the least-squares method. The first approach is the FBS-1 approach, which minimizes the dynamic responses to satisfy the compatibility conditions and transforms them into the frequency domain. The second approach is the FBS-2 approach, which minimizes the FRF matrix to satisfy the compatibility conditions. Because the FRF is closely related to the dynamic characteristics of a structure, it is a crucial factor in establishing the numerical pseudomasses in this study. Numerical examples demonstrate that the FBS-2 approach is a more applicable synthesis technique than the FBS-1 approach. However, an inconsistency in the FRFs between the FBS approaches and analytical analysis was observed. This discrepancy mainly arises from the assumed nonspecifiable pseudomasses and the challenges in describing the low-frequency responses of substructures. Although the FRF curve based on the FBS-2 technique is very close to the analytical FRF curve up to the first resonance frequency, some inconsistencies occur thereafter. Using the FRFs up to the first resonance frequency, this study provides an identification method for estimating the joint parameters based on the FRF variation required to satisfy the compatibility conditions. The validity of the proposed identification method is illustrated using a numerical example.

2. FBS Techniques

Dynamic substructuring for describing the dynamic response of a large structure is derived in the frequency domain. The synthesis was based on the deformation compatibility conditions between adjacent substructures. The compatibility conditions restrict the dynamic responses as constraints, and the synthesis technique modifies the generalized inverse method proposed by Udwadia and Kalaba [27].

2.1. Constrained Dynamic Equation and Dynamic Substructuring. The dynamic equation of motion for a dynamic structure with n DOFs in the time domain can be written as

$$\mathbf{M}\ddot{\mathbf{u}} + \mathbf{C}\dot{\mathbf{u}} + \mathbf{K}\mathbf{u} = \mathbf{f}(t), \tag{1}$$

where $\mathbf{M}$, $\mathbf{C}$, and $\mathbf{K}$ represent the $n \times n$ mass, damping, and stiffness matrices, respectively, whereas $\mathbf{u}$ and $\mathbf{f}$ are the $n \times 1$ displacement and external excitation force vectors, respectively.

Assume that the dynamic behavior of the system is restricted by m linearity and equality conditions, written as

$$\boldsymbol{\phi}(\mathbf{u}, \dot{\mathbf{u}}, t) = \mathbf{0}. \tag{2}$$

Equation (2), when expressed in acceleration components through its time derivative, can be written as

$$\mathbf{A}\ddot{\mathbf{u}} = \mathbf{v}. \tag{3}$$

If the dynamic synthesis of substructures is considered, the coefficient matrix $\mathbf{A}$ denotes the Boolean matrix corresponding to the joint nodes between substructures, and vector $\mathbf{v}$ should be a zero vector.

Using Gauss's principle, the constrained acceleration vector was determined by minimizing the performance index of

$$P = \mathbf{M}^{1/2}(\ddot{\mathbf{q}} - \mathbf{a})\mathbf{M}^{1/2}, \tag{4}$$

where $\ddot{\mathbf{q}}$ and $\mathbf{a}$ are constrained and unconstrained acceleration vectors, respectively. The equations of motion for constrained dynamic systems provided by Udwadia and Kalaba that were used to combine Eqs. (1) and (3) can be expressed as

$$\ddot{\mathbf{q}} = \mathbf{a} + \mathbf{M}^{-1/2}\left(\mathbf{A}\mathbf{M}^{-1/2}\right)^{+}(\mathbf{v} - \mathbf{A}\mathbf{a}), \tag{5}$$

where $\mathbf{a} = -\mathbf{M}^{-1}(\mathbf{C}\dot{\mathbf{u}} + \mathbf{K}\mathbf{u} - \mathbf{f}(t))$. The FRF matrix was derived by transforming the dynamic equations of the synthesized substructures into the frequency domain.

Consider the synthesis of substructures 1 and 2 as shown in Figure 1. The dynamic equation of motion for the two substructures is expressed as follows:

$$\mathbf{M}_{\text{syn}}\ddot{\mathbf{u}}_{\text{syn}} + \mathbf{C}_{\text{syn}}\dot{\mathbf{u}}_{\text{syn}} + \mathbf{K}_{\text{syn}}\mathbf{u}_{\text{syn}} = \mathbf{f}_{\text{syn}} \tag{6}$$

where $\mathbf{M}_{\text{syn}} = \begin{bmatrix} \mathbf{M}_1 & \mathbf{0} \\ \mathbf{0} & \mathbf{M}_2 \end{bmatrix}$, $\mathbf{C}_{\text{syn}} = \begin{bmatrix} \mathbf{C}_1 & \mathbf{0} \\ \mathbf{0} & \mathbf{C}_2 \end{bmatrix}$, $\mathbf{K}_{\text{syn}} = \begin{bmatrix} \mathbf{K}_1 & \mathbf{0} \\ \mathbf{0} & \mathbf{K}_2 \end{bmatrix}$, $\mathbf{u}_{\text{syn}} = \begin{bmatrix} \boldsymbol{u}_1 \\ \boldsymbol{u}_2 \end{bmatrix}$, and $\mathbf{f}_{\text{syn}} = \begin{bmatrix} \mathbf{f}_1 \\ \mathbf{f}_2 \end{bmatrix}$. The subscripts 1 and 2 denote substructures 1 and 2, respectively. The displacement vectors $\mathbf{u}_i\,(i = 1, 2)$ were divided into displacements at the boundary nodes $\mathbf{u}_{ib}$ and displacements at the internal nodes $\mathbf{u}_{ir}$. The subscript "syn" indicates the synthesized substructures containing the full sets of DOFs of the substructures.

The deformation compatibility conditions were used as constraint conditions in the same form as in Eq. (3). The equations of motion for the synthesized structures were obtained by substituting Eqs. (1) and (3) into Eq. (5).

$$\ddot{\mathbf{q}}_{\text{syn}} = \mathbf{a}_{\text{syn}} + \mathbf{M}_{\text{syn}}^{-1/2}\left(\mathbf{A}\mathbf{M}_{\text{syn}}^{-1/2}\right)^{+}\left(\mathbf{v} - \mathbf{A}\mathbf{a}_{\text{syn}}\right), \tag{7}$$

where $\mathbf{a}_{\text{syn}} = -\mathbf{M}_{\text{syn}}^{-1}\left(\mathbf{C}_{\text{syn}}\dot{\mathbf{u}}_{\text{syn}} + \mathbf{K}_{\text{syn}}\mathbf{u}_{\text{syn}} - \mathbf{f}_{\text{syn}}\right)$ and $\mathbf{v} = \mathbf{0}$ in coupling the substructures.

The acceleration vector in Eq. (7) consists of the acceleration components of the boundary and internal nodes. The acceleration components at the joint nodes $\ddot{\mathbf{q}}_{\text{syn},b}$ can be obtained by multiplying the Boolean matrix $\mathbf{B}$, to define the joint nodes.

$$\ddot{\mathbf{q}}_{\text{syn},b} = \mathbf{B}\left[\mathbf{a}_{\text{syn}} + \mathbf{M}_{\text{syn}}^{-1/2}\left(\mathbf{A}\mathbf{M}_{\text{syn}}^{-1/2}\right)^{+}\left(\mathbf{v} - \mathbf{A}\mathbf{a}_{\text{syn}}\right)\right]. \tag{8}$$

The interface forces act on the joint nodes to maintain equilibrium. The forces were obtained by premultiplying the second term on the right-hand side of Eq. (7) using the mass matrix $\mathbf{M}_{\text{syn}}$ as follows:

$$\mathbf{F}^{c} = -\mathbf{M}_{\text{syn}}^{1/2}\left(\mathbf{A}\mathbf{M}_{\text{syn}}^{-1/2}\right)^{+}(\mathbf{v} - \mathbf{A}\mathbf{a}). \tag{9}$$

Because the forces act only on the boundary nodes, they are calculated by premultiplying with the Boolean matrix $\mathbf{B}$. The compatibility conditions are maintained by the action of these forces $\mathbf{F}_b^c$.

$$\mathbf{F}_b^{c} = -\mathbf{B}\mathbf{M}_{\text{syn}}^{-1/2}\left(\mathbf{A}\mathbf{M}_{\text{syn}}^{-1/2}\right)^{+}(\mathbf{v} - \mathbf{A}\mathbf{a}). \tag{10}$$

Equations (7)–(10) express the acceleration components and forces in the time domain. The constrained equations of motion were applied as the basic form of the FBS technique.

2.2. FBS Techniques. Two FBS techniques that depend on the performance index of the least-squares method are derived in this section: (1) synthesizing the dynamic equation in the time domain and then transforming it to the frequency domain and (2) synthesizing the FRFs of each substructure. The synthesis process utilizes the constraints of the compatibility conditions at the interface nodes. The FBS-1 technique in Figure 2 applies the least-squares method to minimize the acceleration variation owing to constraints and utilizes the mass matrix as a weighting matrix. The FBS-2 technique, shown in Figure 3, synthesizes the FRFs of disassembled substructures using compatibility conditions. This technique applies the least-squares method to minimize the variation in the FRF matrices due to constraints with the weighting matrix of the analytical FRF matrix.

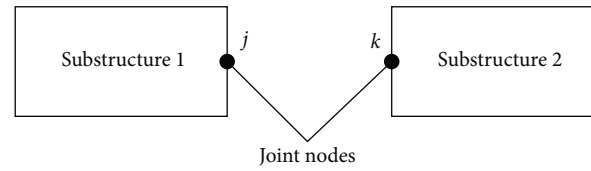

Figure 1: Synthesis of two substructures.

The $s - l\,(l = 1, 2, \cdots, N)$ represents the lth substructure.

2.2.1. FBS-1 Technique. This technique is expressed mathematically to transform the entire synthesized constrained dynamic equation of Eq. (7) in the frequency domain. This method was derived by assuming harmonic excitation. Substituting $\mathbf{u}_{\text{syn}} = \mathbf{U}e^{i\Omega t}$, $\mathbf{f}_{\text{syn}} = \mathbf{F}e^{i\Omega t}$, and $\mathbf{v} = \mathbf{WHF}e^{i\Omega t}$ into Eq. (7) and arranging the result yields

$$-\Omega^2\mathbf{U} = -\mathbf{M}_{\text{syn}}^{-1}\left(i\Omega\mathbf{C}_{\text{syn}}\mathbf{U} + \mathbf{K}_{\text{syn}}\mathbf{U} - \mathbf{F}\right) + \mathbf{M}_{\text{syn}}^{-1/2}\left(\mathbf{A}\mathbf{M}_{\text{syn}}^{-1/2}\right)^{+} \cdot \left(\mathbf{WHF} + \mathbf{A}\mathbf{M}_{\text{syn}}^{-1}\left(i\Omega\mathbf{C}_{\text{syn}}\mathbf{U} + \mathbf{K}_{\text{syn}}\mathbf{U} - \mathbf{F}\right)\right), \tag{11}$$

where $\mathbf{W}$ is the coefficient matrix of the FRF at the nodes related to the harmonic responses and becomes a zero matrix in synthesizing the substructures. The second term on the right side of Eq. (11) indicates the response variations in the frequency domain due to the existence of constraints.

Arranging Eq. (11), it can be expressed by

$$(\mathbf{X} + \mathbf{Y})\mathbf{U} = (\mathbf{I} + \mathbf{R}_1\mathbf{WH} - \mathbf{R})\mathbf{F}, \tag{12}$$

where $\mathbf{I}$ denotes the identity matrix, $\mathbf{X} = -\Omega^2\mathbf{M}_{\text{syn}} + i\Omega\mathbf{C}_{\text{syn}} + \mathbf{K}_{\text{syn}}$, $\mathbf{Y} = -i\Omega\mathbf{R}\mathbf{C}_{\text{syn}} - \mathbf{R}\mathbf{K}_{\text{syn}}$, $\mathbf{R}_1 = \mathbf{M}_{\text{syn}}^{1/2}(\mathbf{A}\mathbf{M}_{\text{syn}}^{-1/2})^{+}$, and $\mathbf{R} = \mathbf{M}_{\text{syn}}^{1/2}(\mathbf{A}\mathbf{M}_{\text{syn}}^{-1/2})^{+}\mathbf{A}\mathbf{M}_{\text{syn}}^{-1}$. The FRF for the dynamic system synthesized from Eq. (12) can be expressed as

$$\mathbf{H}_{\text{cons}} = \frac{\mathbf{I} + \mathbf{R}_1\mathbf{WH} - \mathbf{R}}{\mathbf{X} + \mathbf{Y}}. \tag{13}$$

Equation (13) represents the FRF of the entire coupled structure, including the duplicated FRFs at the interface nodes.

By utilizing the inverse matrix solution for the sum of the two matrices $((\mathbf{A} + \mathbf{B})^{-1} = \mathbf{A}^{-1} - \mathbf{A}^{-1}(\mathbf{B}^{-1} + \mathbf{A}^{-1})\mathbf{A}^{-1})$ to simplify Eq. (13), it can be written as

$$\mathbf{H}_{\text{cons}} = \mathbf{H}\left[\mathbf{I} - \left(\mathbf{Y}^{-1} + \mathbf{H}\right)\mathbf{H}\right](\mathbf{I} + \mathbf{R}_1\mathbf{WH} - \mathbf{R}), \tag{14}$$

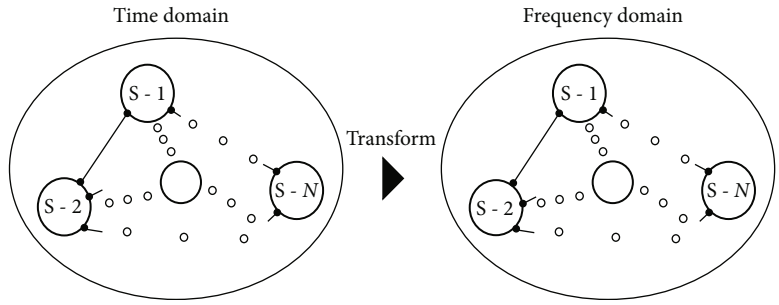

Figure 2: Schematic summary of FBS-1 technique.

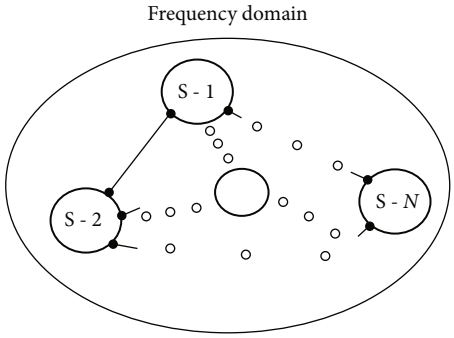

Figure 3: Schematic summary of FBS-2 technique.

where $\mathbf{H}$ denotes the analytical FRF matrix and $\mathbf{H} = \mathbf{X}^{-1}$. Equation (14) is expressed as the sum of the analytical FRFs of the unconstrained finite element model and the FRF variations owing to the compatibility conditions. The FRF variations are expressed as

$$\boldsymbol{\delta}\mathbf{H} = \mathbf{HRB} - \mathbf{HR} - \left[\mathbf{H}\left(\mathbf{Y}^{-1} + \mathbf{H}^{-1}\right)\mathbf{H}\right](\mathbf{I} + \mathbf{R}_1\mathbf{WH} - \mathbf{R}). \tag{15}$$

By premultiplying and postmultiplying both sides of Eq. (14) with the Boolean matrix (to define the interface nodes) and their transpose, respectively, we can write the FRF matrix corresponding to joint nodes j and k in Figure 1 as

$$\mathbf{H}_{\text{cons}}^{jk} = \mathbf{BH}\left[\mathbf{I} - \left(\mathbf{Y}^{-1} + \mathbf{H}^{-1}\right)\mathbf{H}\right](\mathbf{I} + \mathbf{R}_1\mathbf{WH} - \mathbf{R})\mathbf{B}^T. \tag{16}$$

Equation (16) expresses the FRF matrix derived from the constraints of the matching responses at the joint nodes.

2.2.2. FBS-2 Technique. This section derives the FBS-2 technique for constructing the FRFs of s substructures and synthesizing them. The equation of motion for the jth substructure is expressed as

$$\mathbf{M}_j\ddot{\mathbf{u}}_j + \mathbf{C}_j\dot{\mathbf{u}}_j + \mathbf{K}_j\mathbf{u}_j = \mathbf{f}_j(t), \quad j = 1, 2, \cdots, s. \tag{17}$$

We considered the synthesis of the two substructures shown in Figure 3 to simplify the derivation process. The expressions for dividing the two substructures into boundary and internal nodes and transforming the generalized coordinates into modal coordinates are written as

$$\begin{bmatrix} \mathbf{u}_j^i \\ \mathbf{u}_j^b \end{bmatrix} = \begin{bmatrix} \boldsymbol{\phi}_j^i \\ \boldsymbol{\phi}_j^b \end{bmatrix} \mathbf{y}_j, \quad j = 1, 2, \tag{18}$$

where $\boldsymbol{\phi}_j^i$ and $\boldsymbol{\phi}_j^b$ represent the mode-shaped vectors corresponding to the internal and boundary nodes of the jth substructure, respectively. Only a few sets of modes that neglect the higher modes were considered to reduce the DOFs of the synthesized structure, where $\mathbf{u}_j^i$ and $\mathbf{u}_j^b$ represent the displacement vectors at the internal and boundary nodes of the jth substructure, respectively. By substituting Eq. (18) into Eq. (17) and premultiplying with the transpose of the first few mode shape matrices $\boldsymbol{\phi}_j^T (j = 1, 2)$, we obtain the mass-normalized dynamic equations of motion for both substructures as

$$\ddot{\mathbf{y}} + \mathbf{C}^*\dot{\mathbf{y}} + \mathbf{K}^*\mathbf{y} = \mathbf{f}^*, \tag{19}$$

where

$$\mathbf{C}^* = \begin{bmatrix} \mathbf{C}_1^* & \mathbf{0} \\ \mathbf{0} & \mathbf{C}_2^* \end{bmatrix}, \qquad \mathbf{K}^* = \begin{bmatrix} \mathbf{K}_1^* & \mathbf{0} \\ \mathbf{0} & \mathbf{K}_2^* \end{bmatrix} \tag{20}$$

represent the damping and stiffness matrices of the modal reduced-order model

$$\begin{aligned} \mathbf{y} &= \begin{bmatrix} \mathbf{y}_1 \\ \mathbf{y}_2 \end{bmatrix}, \\ \mathbf{C}_j^* &= \boldsymbol{\phi}_j^T\mathbf{C}_j\boldsymbol{\phi}_j, \\ \mathbf{K}_j^* &= \boldsymbol{\phi}_j^T\mathbf{K}_j\boldsymbol{\phi}_j, \\ \mathbf{f}^* &= \begin{bmatrix} \boldsymbol{\phi}_1^T\mathbf{f}_1 \\ \boldsymbol{\phi}_2^T\mathbf{f}_2 \end{bmatrix}, \\ \boldsymbol{\phi}_j &= \begin{bmatrix} \boldsymbol{\phi}_j^i \\ \boldsymbol{\phi}_j^b \end{bmatrix}. \end{aligned} \tag{21}$$

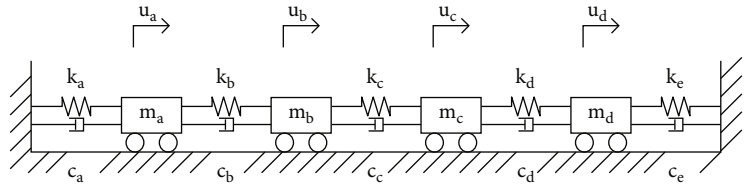

Figure 4: A four-DOF system.

The compatibility conditions between two substructures can be written by

$$\mathbf{u}_1^b = \mathbf{u}_2^b \text{ or} \tag{22}$$

$$\boldsymbol{\phi}_1^b \mathbf{y}_1 = \boldsymbol{\phi}_2^b \mathbf{y}_2. \tag{23}$$

The compatibility conditions in Eq. (22) can be written in matrix form using the generalized and modal coordinates, as follows:

$$\mathbf{A}_1 \mathbf{u} = \mathbf{0} \text{ or} \tag{24}$$

$$\mathbf{A}\mathbf{y} = \mathbf{0}. \tag{25}$$

Inserting $\mathbf{y} = \mathbf{Y}e^{i\Omega t}$ and $\mathbf{f}^* = \mathbf{F}^* e^{i\Omega t}$ into Eqs. (19) and (24) can be expressed as follows:

$$\mathbf{K}_d \mathbf{Y} = \mathbf{F}^*, \tag{26a}$$

$$\mathbf{A}\mathbf{Y} = \mathbf{0}, \tag{26b}$$

where

$$\mathbf{K}_d = \mathbf{H}_d^{-1} = \begin{bmatrix} -\Omega^2\mathbf{I} + i\Omega\mathbf{C}_1^* + \Omega\mathbf{K}_1^* & \mathbf{0} \\ \mathbf{0} & -\Omega^2\mathbf{I} + i\Omega\mathbf{C}_2^* + \Omega\mathbf{K}_2^* \end{bmatrix},$$

$$\mathbf{Y} = \begin{bmatrix} \mathbf{Y}_1 \\ \mathbf{Y}_2 \end{bmatrix},$$

$$\mathbf{F}^* = \begin{bmatrix} \mathbf{F}_1^* \\ \mathbf{F}_2^* \end{bmatrix}. \tag{27}$$

$\mathbf{K}_d$ is the dynamic stiffness matrix in the frequency domain and its inverse is the FRF matrix.

The dynamic equation owing to the constraints, such as Eq. (24), is determined by minimizing the performance index of

$$\mathrm{P}_\Omega = \mathbf{H}_d^{-1/2}(\mathbf{H}_{d\_\mathrm{con}} - \mathbf{H}_d)\mathbf{H}_d^{-1/2}. \tag{28}$$

By using $\mathbf{H}_d^{-1/2}(\mathbf{H}_d^{1/2}) = \mathbf{I}$ in Eq. (26b) and replacing $\mathbf{M}_{\mathrm{syn}}$ in Eq. (7) by $\mathbf{H}_d^{-1}$, the dynamic equation in the frequency domain can be written as

$$\mathbf{Y} = \widehat{\mathbf{Y}} - \mathbf{H}_d^{1/2}\left(\mathbf{A}\mathbf{H}_d^{1/2}\right)^+ \mathbf{A}\widehat{\mathbf{Y}} \text{ or} \tag{29}$$

$$\mathbf{Y} = \left(\mathbf{I} - \mathbf{H}_d^{1/2}\left(\mathbf{A}\mathbf{H}_d^{1/2}\right)^+ \mathbf{A}\right)\mathbf{H}_d\mathbf{F}^*, \tag{30}$$

where $\widehat{\mathbf{Y}} = \mathbf{H}_d\mathbf{F}^*$. Thus, the FRF matrix of the synthesized structure, $\mathbf{H}_{d\_\mathrm{con}}$, can be expressed as

$$\mathbf{H}_{d\_\mathrm{con}} = \left(\mathbf{I} - \mathbf{H}_d^{1/2}\left(\mathbf{A}\mathbf{H}_d^{1/2}\right)^+ \mathbf{A}\right)\mathbf{H}_d. \tag{31}$$

Equation (31) represents the FRF matrix of the entire coupled structure used to synthesize the FRFs of the substructures, unlike Eq. (14). If the constraints are given in the form of Eq. (3), the FRF matrix was modified as follows:

$$\mathbf{H}_{d\_\mathrm{con}} = \mathbf{H}_d - \mathbf{H}_d^{1/2}\left(\mathbf{A}\mathbf{H}_d^{1/2}\right)^+ (\mathbf{W} - \mathbf{A})\mathbf{H}_d. \tag{32}$$

Equation (32) expresses the FRF matrix synthesized using the FRFs of the substructures as constraints. It can be observed that Eqs. (14) and (32) take different forms of the FRF matrices depending on the constraints.

2.3. Estimation of Connector Parameters. The physical parameters of the connectors linking the substructures can be predicted through the interface forces, as these forces describe the additional requirements to satisfy the constraints. They are derived using the inverse relationship between the dynamic stiffness matrix and FRF matrix. The physical parameters of the connectors were estimated using the FRFs at the joint nodes of each substructure before and after synthesis.

By considering the interfacial forces in Eq. (9) to act on the substructure, and excluding external harmonic excitations in the frequency domain, we can write the equation as

$$\left(-\Omega^2\mathbf{M}_{\mathrm{syn}} + i\Omega\mathbf{C}_{\mathrm{syn}} + \mathbf{K}_{\mathrm{syn}}\right)\mathbf{U} = \mathbf{M}_{\mathrm{syn}}^{1/2}\left(\mathbf{A}\mathbf{M}_{\mathrm{syn}}^{-1/2}\right)^+ \mathbf{A}\mathbf{M}_{\mathrm{syn}}^{-1}\left(i\Omega\mathbf{C}_{\mathrm{syn}}\mathbf{U} + \mathbf{K}_{\mathrm{syn}}\mathbf{U} - \mathbf{F}\right). \tag{33}$$

Equation (33) is related to the forces that represent the variations in the responses before and after the constraints are imposed. By substituting $\mathbf{R} = \mathbf{M}_{\mathrm{syn}}^{1/2}(\mathbf{A}\mathbf{M}_{\mathrm{syn}}^{-1/2})^+ \mathbf{A}\mathbf{M}_{\mathrm{syn}}^{-1}$ into Eq. (33) and arranging the result yields

$$\mathbf{U} = \mathbf{H}_{\mathrm{con}}\mathbf{F}, \tag{34}$$

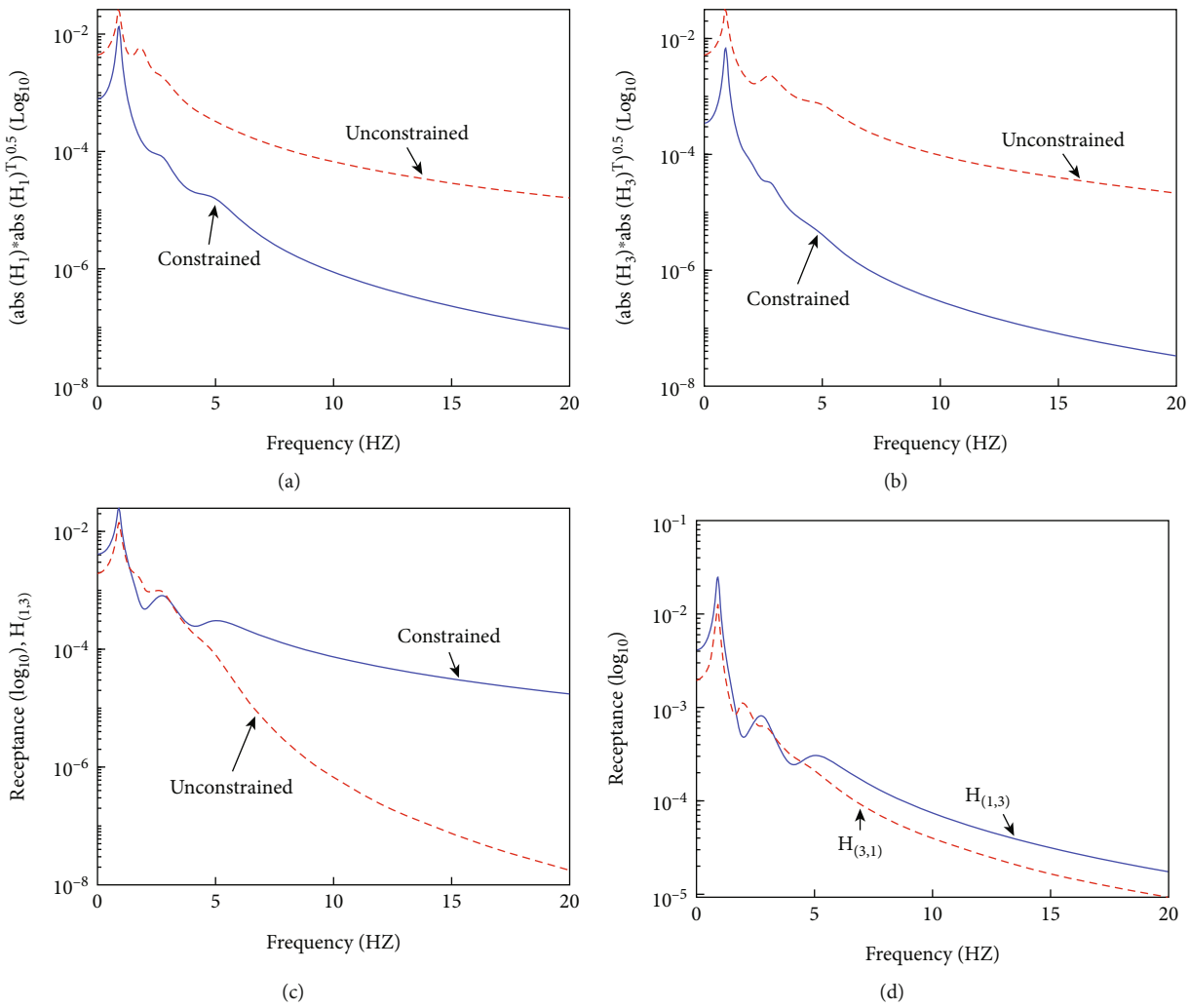

FIGURE 5: Comparison of FRF receptance curves of constrained and unconstrained systems: (a) SRSS of the first row of FRF matrix corresponding to U_a, (b) SRSS of the third row of FRF matrix corresponding to U_c, (c) receptance curve of $H_{1,3}$, and (d) receptance curves of $H_{1,3}$ and $H_{3,1}$.

where $\mathbf{H}_{con} = -\mathbf{R}/((-\Omega^2\mathbf{M}_{syn} + i\Omega\mathbf{C}_{syn} + \mathbf{K}_{syn}) - \mathbf{R}(i\Omega\mathbf{C}_{syn}\mathbf{U} + \mathbf{K}_{syn}\mathbf{U}))$. $\mathbf{H}_{con}$ on the left-hand side of Eq. (34) represents the FRFs measured numerically or experimentally at the joint nodes of a coupled structure.

Letting $\mathbf{Q} = (-\Omega^2\mathbf{M}_{syn} + i\Omega\mathbf{C}_{syn} + \mathbf{K}_{syn})$ and $\mathbf{E} = -\mathbf{R}(i\Omega\mathbf{C}_{syn} + \mathbf{K}_{syn})$ in the denominator in the right-hand side of Eq. (34), utilizing the inverse matrix solution for the sum of the two matrices, and arranging the result yields

$$\mathbf{H}_{con} = \left[\mathbf{Q}^{-1} - \mathbf{Q}^{-1}\left\{\mathbf{E}^{-1} + \mathbf{Q}^{-1}\right\}^{-1}\mathbf{Q}^{-1}\right]\mathbf{R}, \quad (35)$$

where the right side of Eq. (35) only represents the FRFs corresponding to the joint nodes. Inserting $\mathbf{H} = \mathbf{Q}^{-1}$ into Eq. (35) and solving the result with respect to the parameters, we obtain

$$\mathbf{R}(i\Omega\mathbf{C} + \mathbf{K}) = \left[\mathbf{H} - \mathbf{H}\left\{\mathbf{I} + \mathbf{H}^{-1}\mathbf{H}_{con}\mathbf{R}^{-1}\right\}^{-1}\right]^{-1}, \quad (36)$$

where the parameter matrices and the FRF matrix include the effect of rotational DOFs and they should be considered.

It was assumed that the mass at the interface nodes was not a parameter to be estimated. The values on the right side of Eq. (36) from Ω_1 to Ω_h are divided into real and imaginary parts, and the equations for the parameter matrices are written by

$$\begin{bmatrix} \mathbf{R}(\Omega_1) & \mathbf{0} \\ \mathbf{0} & \Omega_1\mathbf{R}(\Omega_1) \\ \mathbf{R}(\Omega_2) & \mathbf{0} \\ \mathbf{0} & \Omega_2\mathbf{R}(\Omega_2) \\ \vdots & \vdots \\ \mathbf{R}(\Omega_h) & \mathbf{0} \\ \mathbf{0} & \Omega_h\mathbf{R}(\Omega_h) \end{bmatrix} \begin{bmatrix} \mathbf{K} \\ \mathbf{C} \end{bmatrix} = \begin{bmatrix} \text{real}(\text{FRF}(\Omega_1)) \\ \text{imag}(\text{FRF}(\Omega_1)) \\ \text{real}(\text{FRF}(\Omega_2)) \\ \text{imag}(\text{FRF}(\Omega_2)) \\ \vdots \\ \text{real}(\text{FRF}(\Omega_h)) \\ \text{real}(\text{FRF}(\Omega_h)) \end{bmatrix}. \quad (37)$$

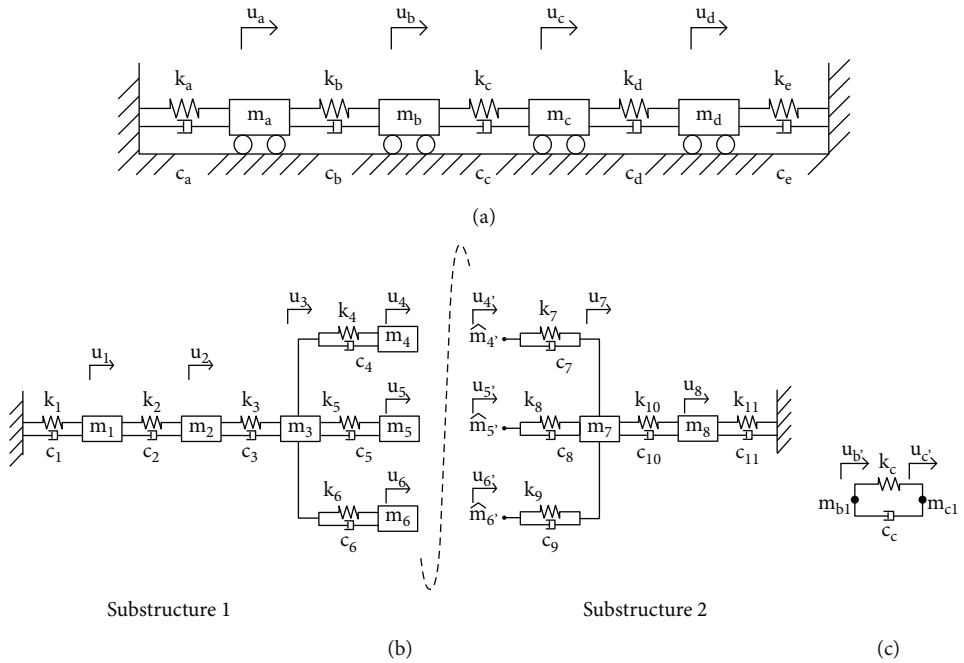

FIGURE 6: Decoupled substructures of a four-DOF structure: (a) entire structure, (b) substructures 1 and 2, and (c) substructure 3.

Solving Eq. (37), using the pseudoinverse with respect to the parameter matrices, yields

$$\begin{bmatrix} \mathbf{K} \\ \mathbf{C} \end{bmatrix} = \begin{bmatrix} \mathbf{R}(\Omega_1) & \mathbf{0} \\ \mathbf{0} & \Omega_1\mathbf{R}(\Omega_1) \\ \mathbf{R}(\Omega_2) & \mathbf{0} \\ \mathbf{0} & \Omega_2\mathbf{R}(\Omega_2) \\ \vdots & \vdots \\ \mathbf{R}(\Omega_h) & \mathbf{0} \\ \mathbf{0} & \Omega_h\mathbf{R}(\Omega_h) \end{bmatrix}^{+} \begin{bmatrix} \text{real}(\text{FRF}(\Omega_1)) \\ \text{imag}(\text{FRF}(\Omega_1)) \\ \text{real}(\text{FRF}(\Omega_2)) \\ \text{imag}(\text{FRF}(\Omega_2)) \\ \vdots \\ \text{real}(\text{FRF}(\Omega_h)) \\ \text{real}(\text{FRF}(\Omega_h)) \end{bmatrix}. \tag{38}$$

The solution of Eq. (38) yields the stiffness and damping parameters of the connectors. The results can be expanded to techniques for predicting the joint parameter matrices to connect three or more substructures.

3. Numerical Examples

3.1. FBS Approaches of Four DOF Systems. Consider the finite element model with four DOFs shown in Figure 4. This example estimates the updated FRFs of the system because of a constraint that restricts the relative responses in the frequency domain. The physical properties used in this example, neglecting the units, are assumed to be as follows: $m_a = 4$, $m_b = 2$, $m_c = 3$, $m_d = 5$, $k_a = 220$, $k_b = 450$, $k_c = 880$, $k_d = 480$, $k_e = 270$, $c_a = 4.4$, $c_b = 8$, $c_c = 9$, $c_d = 7$, and $c_e = 10$.

This example describes the FRFs of a dynamic system constrained by the displacement relationship, $\mathbf{AU} = \mathbf{WHF}$. It is written by $U_a - 0.8U_c = [0\,0\,0.7\,0]\mathbf{HF}$, where $\mathbf{A} = [1\,0 - 0.8\,0]$ and $\mathbf{W} = [0\,0\,0.7\,0]$.

By substituting the constraint and dynamic equation of the system in the frequency domain into Eq. (32), the constrained FRFs were explicitly obtained.

The FRFs were numerically calculated using the FRF-2 technique from 0.01 Hz to 20 Hz in 0.02 Hz increments. Figures 5(a) and 5(b) show the square root of the sum of squares (SRSS) of the entire FRFs of nodal displacements U_a and U_c within the corresponding frequency range before and after applying the constraint, respectively. The difference between the two curves indicates that the FRF variations deviate from the initial responses to satisfy the constraint. It was evaluated that the displacements U_a and U_c satisfy the constraint. The constrained FRF curves deviate from the unconstrained curves owing to these constraints.

Figure 5(c) compares the FRF receptances of $H_{1,3}$ in the constrained and unconstrained states where $H_{x,y}$ represents the response at node x to the excitation at node y. A difference in the FRFs between the constrained and unconstrained states is observed, and it increases with an increase in frequency. The symmetry of the FRF receptance matrix due to this constraint was investigated. It can be observed from Figure 5(d) that the two curves of $H_{1,3}$ and $H_{3,1}$ are inconsistent and therefore do not maintain symmetry. The FRF curves can be obtained explicitly using the proposed FBS approach without any numerical scheme.

The next example considers the synthesis of the three substructures, as shown in Figure 6. The synthesis was performed using the two techniques presented in this study. Substructure 1 is depicted by the displacement DOFs of u_a

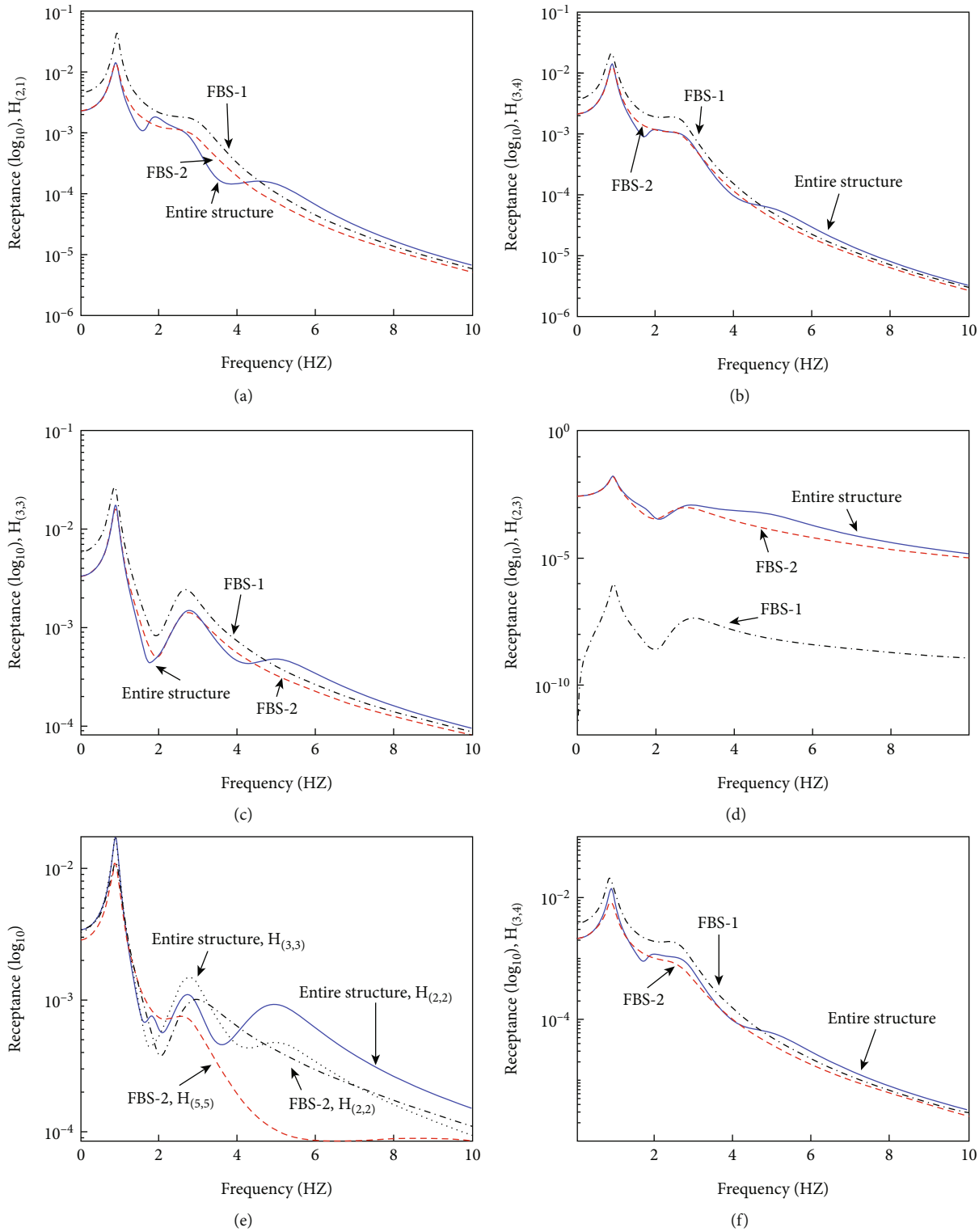

FIGURE 7: Comparison of numerical results of FBS-1, FBS-2, and intact FRFs: (a) $H_{2,3}$, (b) $H_{3,4}$, (c) $H_{3,3}$, (d) $H_{2,1}$, (e) FRF receptance at joint nodes, and (f) FRF receptance of pseudomass 0.5.

and u_b, substructure 2 by u_c and u_d, and substructure 3 by $u_{b'}$ and $u_{c'}$, respectively. Substructures 1 and 2 are supported by fixed ends, whereas substructure 3 is a floating structure without support ends. The FBS techniques presented in this study require pseudomasses at the joint nodes for a full-rank mass matrix. The FBS approaches were developed by

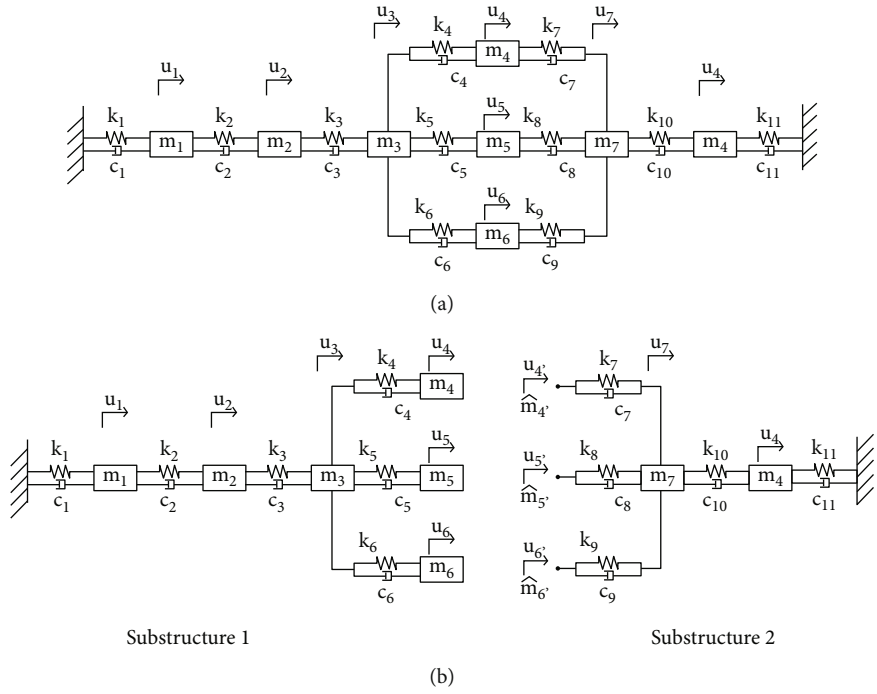

Figure 8: Model of example 2: (a) entire structure and (b) two substructures.

assuming the values of the pseudomasses at the joint nodes. The pseudomasses affect the dynamic characteristics of each substructure. Thus, the influences of the pseudomasses were numerically compared in this example.

Assuming very small pseudomasses of magnitude 0.0001 at both ends of substructure 3, Figures 7(a)–7(c) compare the FRF receptance curves determined using the FBS-1 and FBS-2 approaches and the analytical FRF receptance curve of the entire structure. Subscripts 1, 2, 3, 4, 5, and 6 correspond to the displacement DOFs u_a, u_b, u_c, u_d, $u_{b'}$, and $u_{c'}$, respectively. The numerical results obtained using the proposed FBS techniques were inconsistent with the frequency analysis results for the entire structure. It was confirmed that the discrepancy was reduced in the frequency region greater than 10 Hz but was maintained at a certain value. This inconsistency is likely caused by the different constraint forms of displacement, FRF, and assumed pseudomasses and is attributed to the unclear modal characteristics of floating substructure 3, owing to the unknown pseudomasses. The FBS-2 technique exhibits a smaller discrepancy than the FBS-1 approach. The FBS-2 technique was almost identical to the precise solution up to the first resonance frequency. The discrepancy in higher frequency regions is likely due to the unclear modal characteristics of substructure 3. Figure 7(d) shows the FRF $H_{2,3}$ curve related to nodal displacement u_b of substructure 1 owing to the input at nodal displacement u_c of substructure 2. The FBS-1 technique exhibits a large discrepancy because the input and output nodes are located in different substructures. It is predicted that the FBS-1 technique can only be utilized for local synthesis with the input and output nodes in the same substructure.

Figure 7(e) compares the FRFs of $H_{2,2}$ and $H_{5,5}$, $H_{3,3}$, and $H_{6,6}$ of the joint nodes determined using the FBS-2 technique. The compatibility conditions do not restrict each element of the FRF matrix but only constrain the displacements at interface nodes. Thus, even if the nodal displacements are identical, the elements of the FRF matrix rarely appear to be identical. The FRF curves exhibit very similar forms or contain small errors up to the first resonance frequency; however, after that, the forms and errors are significantly different. The difference in the FRF curves according to the change in the pseudomasses is compared in Figure 7(b) for a pseudomass of 0.0001 and Figure 7(f) for a pseudomass of 0.5. Despite the increase in pseudomasses to 0.5, the FRF curves showed no significant changes. More in-depth research is required to improve the method for describing the behavior in the low-frequency range of substructure 2, which is a floating structure.

3.2. FBS Approaches of Substructure with Several Interface Nodes. Figure 8(a) exhibits a structure that is a composite of two substructures in Figure 8(b). This example considers the synthesis of two substructures using the FBS-2 technique, as shown in Figure 8(a). Substructure 1 consisted of six displacement DOFs of u_1, u_2, u_3, u_4, u_5, and u_6 set to 1, 2, 3, 4, 5, and 6, respectively. Substructure 2 consisted of five displacement DOFs of $u_{4'}$, $u_{5'}$, $u_{6'}$, u_7, and u_8 set to 7, 8, 9, 10, and 11, respectively. The compatibility conditions of the two substructures can be written as $u_4 = u_{4'}$, $u_5 = u_{5'}$, and $u_6 = u_{6'}$.

The FBS-2 technique was applied, assuming a pseudomass of 0.001 at the joint nodes of substructure 2. The parameter values of the structure are assumed to be $m_1 = 3$,

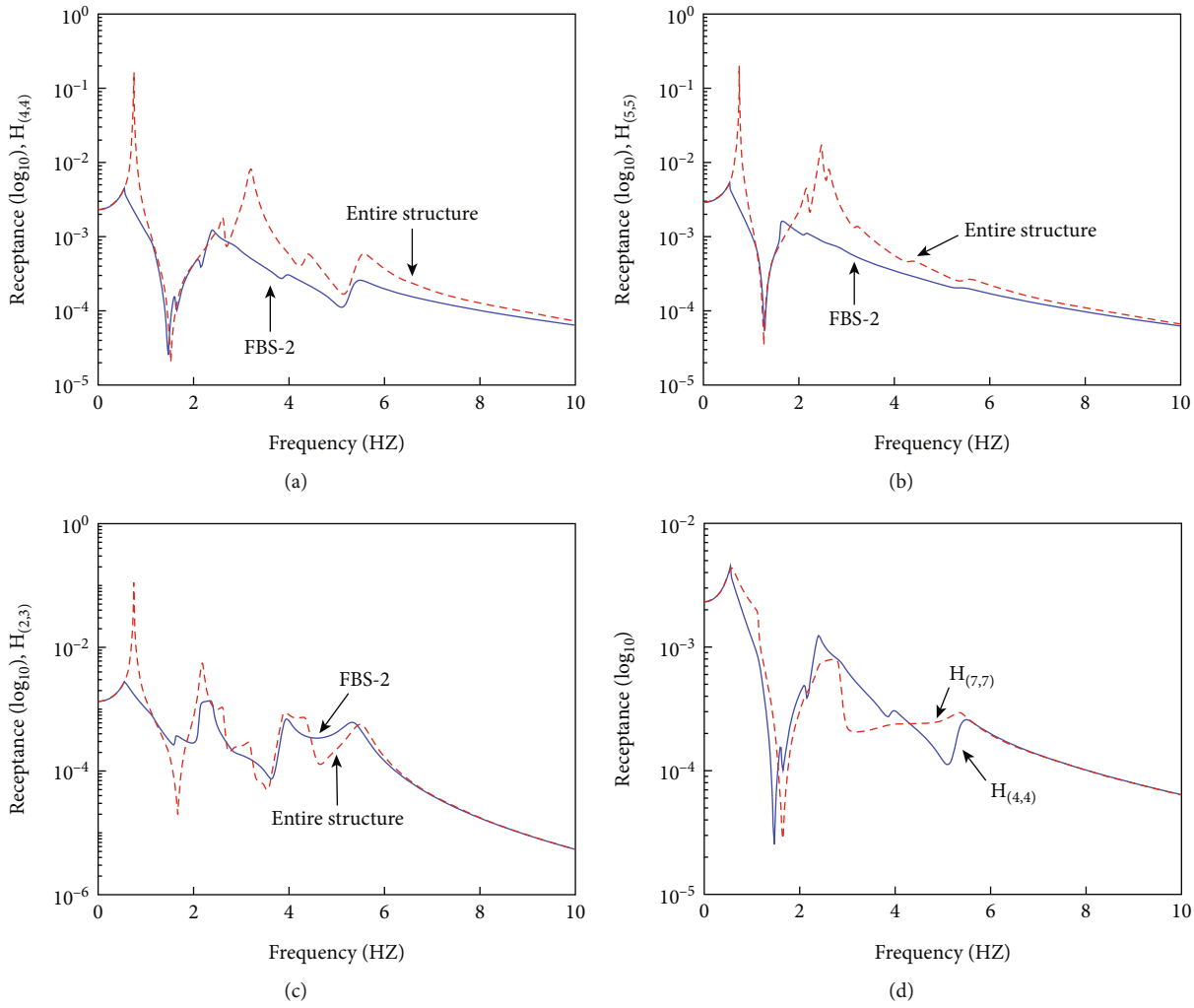

Figure 9: Comparison of FRF receptance curves of FBS and entire structure: (a) $H_{4,4}$, (b) $H_{5,5}$, (c) $H_{2,3}$, (d) $H_{4,4}$, and $H_{7,7}$.

$m_2 = 4$, $m_3 = 3$, $m_4 = 4$, $m_5 = 4$, $m_6 = 5$, $m_7 = 5$, $m_8 = 5$, $k_1 = 880$, $k_2 = 830$, $k_3 = 690$, $k_4 = 1020$, $k_5 = 360$, $k_6 = 730$, $k_7 = 920$, $k_8 = 550$, $k_9 = 940$, $k_{10} = 570$, and $k_{11} = 720$.

By inserting the FRFs of the two substructures and the compatibility conditions in the frequency domain into Eq. (31), the FRFs of the synthesized structures were determined. As shown in Figures 9(a)–9(c), the results synthesized using the FBS-2 algorithm rarely match the analytical FRFs of the entire structure. They almost match the first resonance frequency region, but an inconsistency occurs in the subsequent frequency. The errors are likely caused by the unclear modal characteristics of the substructure, resulting from the assumed pseudomasses. This suggests that the system identification or substructure synthesis can effectively utilize FRF data up to the first resonance frequency region. Compatibility conditions at the joint nodes must be satisfied. The FRFs at the joint nodes are compared in Figure 9(d). An inconsistency between the two curves was observed. Equation (31) is derived under the precondition that the displacement constraints rather than the FRFs must be satisfied. Thus, it is concluded that the discrepancy is caused by the FRFs, which is consistent with the influence of the modal characteristics owing to the pseudomasses.

3.3. Identification of Joint Parameters. This example considers the estimation of the joint parameters of the system, as shown in Figure 6. The measurement data used are the FRFs collected from numerical experiments, ranging from 0.01 Hz to 2 Hz at 0.02 Hz intervals, including the first resonance frequency. The parameter values of the connector were estimated using the measured FRFs at the joint nodes of the two independent substructures, the coupled entire structure, and the compatibility conditions. The parameters can be calculated from the interface forces between the two substructures and the connector because they are related to the variation in the FRF during synthesis. These parameters were estimated using Eq. (38).

The FRFs of the two independent substructures, 1 and 2, and the FRFs of the entire structure in Figure 6 were extracted at the same joint nodes. The measured FRFs

contain external noise. The measured FRFs containing noise effects were numerically simulated as

$$\mathbf{D} = \mathbf{D}_o(\mathbf{I} + \alpha\sigma), \tag{39}$$

where α denotes the relative magnitude of the error and σ is a random number variant in the range $[-1, 1]$. This example considers the relative magnitude of the error as 0.1.

The parameter values of the connector using Eq. (38) were predicted by dividing them into noise-free and 10% noise-free cases. The resulting values were obtained as follows:

(1) Noise-free

$$\mathbf{K}_{s-2} = \begin{bmatrix} 1588.2 & -880 \\ -880 & 2665.4 \end{bmatrix}, \quad \mathbf{C}_{s-2} = \begin{bmatrix} 54.2 & -9.0 \\ -9.0 & 92.5 \end{bmatrix}. \tag{40}$$

(2) 10% noise magnitude

$$\mathbf{K}_{s-2} = \begin{bmatrix} 1588.4 & -884.4 \\ -876.3 & 2659.6 \end{bmatrix}, \quad \mathbf{C}_{s-2} = \begin{bmatrix} 53.6 & -9.05 \\ -8.97 & 92.0 \end{bmatrix}. \tag{41}$$

Despite the presence of external noise, it was confirmed that the proposed identification technique could appropriately estimate the physical properties of the connector. The proposed method can explicitly predict the joint parameters based on variations in the FRFs.

4. Conclusions

In this study, the synthesis of substructures in the frequency domain was considered. The synthesis utilized deformation compatibility conditions at the interface nodes between adjacent substructures. Using modal coordinates, such as in the CMS technique, reduces the number of DOFs of the structure and allows for the synthesis of explicit expressions without the need for a Lagrange multiplier. An identification approach for joint parameters to join substructures was provided. The results of this study are summarized as follows.

(1) Two FBS techniques, FBS-1 and FBS-2, were used for dynamic substructuring according to the performance indices. The FBS techniques are presented in an explicit form without any numerical schemes

(2) Inconsistencies between the analytical FRFs and FRFs determined using the proposed methods were observed. It was found that the main cause of the discrepancy was the difficulty in describing the low-frequency responses owing to the nonspecifiable pseudomasses of the substructures. It was determined that it is necessary to model the joints and analyze the joint nodes to describe their behavior in the low-frequency range of the substructure

(3) When the input and output nodes exist within the same substructure, FBS-1 exhibits larger errors than FBS-2. The analysis results using the FBS-2 technique were almost identical up to the first resonance frequency, but the errors increased slightly in subsequent regions. FBS-1 exhibits significantly different results when the input and output nodes are located at the nodes of different substructures

(4) This study provides an identification method for estimating joint parameters based on the FRF variation. The joint parameters were explicitly estimated using the FRF variations owing to the compatibility conditions

Data Availability

The data used to support the findings of this study are included within the article.

Conflicts of Interest

The authors declare that they have no known competing financial interests or personal relationships that could have appeared to influence the work reported in this paper.

Acknowledgments

This study has been worked with the support of a research grant of Kangwon National University in 2023. This research was supported by Basic Science Research Program through the National Research Foundation of Korea (NRF) funded by the Ministry of Education (RS-2023-00242973).

References

[1] B. Jetmundsen, R. Bielawa, and W. Flannelly, "Generalized frequency domain substructure synthesis," *Journal of the American Helicopter Society*, vol. 33, no. 1, pp. 55–64, 1988.

[2] T. A. N. Silva and N. M. M. Maia, "Estimation of rotational frequency response functions," *Special Topics in Structural Dynamics*, vol. 6, 2015.

[3] N. M. M. Maia and T. A. N. Silva, "An expansion technique for the estimation of unmeasured rotational frequency response functions," *Mechanical Systems and Signal Processing*, vol. 156, article 107634, 2021.

[4] F. C. Batista and N. M. M. Maia, *Estimation of unmeasured frequency response functions*, ICSV19, 2012.

[5] W. I. I. Wan Iskandar Mirza, M. N. Abdul Rani, M. A. Yunus, D. Stancioiu, and V. Shripathi, "Estimating rotational frequency response function using mode expansion and

frequency response function synthesis method," *International Journal of Automotive and Mechanical Engineering*, vol. 18, no. 2, pp. 8738–8750, 2021.

[6] N. Hosoya and T. Yoshimura, "Estimation of frequency response function on rotational degrees of freedom of structures," *International Design Engineering Technical Conferences and Computers and Information in Engineering Conference*, vol. 19760, pp. 169–174, 2021.

[7] X. Yang, X. Guo, H. Ouyang, and D. Li, "A new frequency matching technique for FRF-based model updating," *Journal of Physics: Conference Series*, vol. 842, no. 1, article 012013, 2017.

[8] T. A. N. Silva, N. M. M. Maia, and J. I. Barbosa, "A model updating technique based on FRFs for damped structures," in *International Conference on Noise and Vibration Engineering (ISMA)*, pp. 2213–2226, Katholieke Univ Leuven, Belgium, 2012.

[9] Y. Wu, R. Zhu, Z. Cao, Y. Liu, and D. Jiang, "Model updating using frequency response functions based on Sherman-Morrison formula," *Applied Sciences*, vol. 10, no. 4, 2020.

[10] E. Jamshidi, M. R. Ashory, A. Ghoddosian, and N. Nematipoor, "FRF-based model updating using SMURF technique," *Journal of Vibroengineering*, vol. 14, no. 2, pp. 637–650, 2012.

[11] J. Harvie and P. Avitabile, "Effects of precise FRF measurements for frequency based substructuring," *Sound and Vibration*, vol. 52, no. 1, 2018.

[12] F. Shadan, F. Khoshnoudian, D. J. Inman, and A. Esfandiari, "Experimental validation of a FRF-based model updating method," *Journal of Vibration and Control*, vol. 24, no. 8, 2016.

[13] R. A. Patil, "Joint parameter determination using FRF decoupling method for connected solid plates," *Journal of Physics: Conference Series*, vol. 1896, no. 1, article 012015, 2021.

[14] A. Drozg, G. Cepon, and M. Boltezar, "Full-degrees-of-freedom frequency based substructuring," *Mechanical Systems and Signal Processing*, vol. 98, pp. 570–579, 2018.

[15] D. De Klerk, D. Rixen, and J. Jong, "The frequency based substructuring method reformulated according to the dual domain decomposition method," in *Proceedings of the 24th International Modal Analysis Conference, A Conference on Structural Dynamics*, St. Louis, MO, 2006.

[16] A. E. Mahmoudi, D. J. Rixen, and C. H. Meyer, "Comparison of different approaches to include connection elements into frequency-based substructuring," *Experimental Techniques*, vol. 44, no. 4, pp. 425–433, 2020.

[17] M. Bouslema, T. Fakhfakh, R. Nasri, and M. Haddar, "The effect of perturbation on the FRF based substructuring," in *Mechatronics 4.0: Proceedings Of The First International Workshop On Mechatronics 4.0, June 8–9, 2019, Mahdia, Tunisia 4.0*, pp. 145–152, Springer International Publishing, 2020.

[18] M. Law and S. Ihlenfeldt, "A frequency-based substructuring approach to efficiently model position-dependent dynamics in machine tools," *Journal of Multi-body Dynamics*, vol. 229, no. 3, pp. 304–317, 2014.

[19] H. Jalali, "Linear contact interface parameter identification using dynamic characteristic equation," *Mechanical Systems and Signal Processing*, vol. 66-67, pp. 111–119, 2016.

[20] Y. Yang, J. Chen, F. Lan, F. Xiong, and Z. Zeng, "Joints parameters identification in numerical modeling of structural dynamics," *Shock and Vibration*, vol. 2018, Article ID 2365759, 11 pages, 2018.

[21] M. Sanati, Y. Alammari, J. H. Ko, and S. S. Park, "Identification of joint dynamics in lap joints," *Archive of Applied Mechanics*, vol. 87, no. 1, pp. 99–113, 2017.

[22] T. Yang, S.-H. Fan, and C.-S. Lin, "Joint stiffness identification using FRF measurements," *Computers & Structures*, vol. 81, no. 28-29, pp. 2549–2556, 2003.

[23] D.-H. Lee and W.-S. Hwang, "An identification method for joint structural parameters using an FRF-based substructuring method and an optimization technique," *Journal of Mechanical Science and Technology*, vol. 21, no. 12, pp. 2011–2022, 2007.

[24] K.-T. Yang and Y.-S. Park, "Joint structural parameter identification using a subset of frequency response function measurements," *Mechanical Systems and Signal Processing*, vol. 7, no. 6, pp. 509–530, 1993.

[25] H. Y. Hwang, "Identification techniques of structure connection parameters using frequency response functions," *Journal of Sound and Vibration*, vol. 212, no. 3, pp. 469–479, 1998.

[26] W. L. Li, "A new method for structural model updating and joint stiffness identification," *Mechanical Systems and Signal Processing*, vol. 16, no. 1, pp. 155–167, 2002.

[27] F. E. Udwadia and R. E. Kalaba, "A new perspective on constrained motion," *Proceedings. Royal Society of London*, vol. 439, no. 1906, pp. 407–410, 1992.